1-1-2009

Quantification of L1(0) phase volume fraction in annealed Fe/Pt (n) multilayer films

Bo Yao
University of Central Florida

Kevin R. Coffey
University of Central Florida

Journal of Applied Physics

Quantification of $L1_0$ phase volume fraction in annealed $[Fe/Pt]_n$ multilayer films

Cite as: J. Appl. Phys. **105**, 033901 (2009); https://doi.org/10.1063/1.3068364
Submitted: 05 September 2008 . Accepted: 05 December 2008 . Published Online: 02 February 2009

Bo Yao, and Kevin R. Coffey

Quantification of $L1_0$ phase volume fraction in annealed $[Fe/Pt]_n$ multilayer films

Bo Yao[a] and Kevin R. Coffey
Advanced Materials Processing and Analysis Center and Department of Mechanical, Materials and Aerospace Engineering, University of Central Florida, Orlando, Florida 32816, USA

(Received 5 September 2008; accepted 5 December 2008; published online 2 February 2009)

The heat treatment of $[Fe/Pt]_n$ multilayer films is a promising approach to form the $L1_0$ FePt phase at a reduced temperature, which is of interest for applications as high-density magnetic recording media and high-energy permanent magnets. The volume fraction of the $L1_0$ FePt phase in the annealed films strongly influences their magnetic properties. This paper introduces a novel method based on hollow cone dark field transmission electron microscopy imaging to quantify the $L1_0$ FePt phase volume fraction. This method is used to characterize two sets of $[Fe/Pt]_n$ multilayer films with varying deposition temperature and periodicity. It was found that both the deposition temperature and bilayer periodicity are significant to the structure and magnetic properties of annealed films and to the extent to which the $L1_0$ phase is formed. A correlation between $L1_0$ phase volume fraction, grain size, and magnetic properties was also observed. © *2009 American Institute of Physics*.
[DOI: 10.1063/1.3068364]

I. INTRODUCTION

The ordered $L1_0$ FePt phase has potential applications for high-density magnetic recording media and high-energy permanent magnets due to its large magnetocrystalline anisotropy energy density ($K_u \sim 7 \times 10^7$ ergs/cm^3), high Curie temperature (~480 °C), and large saturation magnetization ($\mu_0 M_s \sim 1.43$ T).[1] FePt films with the stoichiometric composition of 50 at. % Fe that are deposited at room temperature have a disordered fcc structure, which has a low anisotropy energy density and therefore lacks attractive hard magnetic properties. Postannealing at high temperature is necessary to induce the disorder (fcc) to order ($L1_0$) phase transformation, and a mixture of both the disordered fcc and ordered $L1_0$ phases is commonly observed in the annealed films. While both the volume fraction of the $L1_0$ phase and the extent of chemical order within the $L1_0$ phase are important to magnetic properties, this work focuses on a novel technique to measure the volume fraction of the $L1_0$ phase present in thin film samples. Clearly magnetic recording media applications will require full transformed samples (100% $L1_0$ phase). Permanent magnet application may utilize intermediate volume fractions of the $L1_0$ phase in exchange-spring magnets. Further, the quantification of the volume fraction of the $L1_0$ phase is important to the development of our understanding of the kinetics of this solid state reaction in thin films. The heat treatment of $[Fe/Pt]_n$ multilayer thin films is a promising approach to form the $L1_0$ FePt phase at a reduced temperature, which is highly desirable for many of the applications. Although the mechanism of diffusion and reaction of $[Fe/Pt]_n$ multilayers is not completely clear, the magnetic properties of annealed multilayers suggest that they are also mixtures of fcc and $L1_0$ FePt phases.[2]

The volume fraction of the $L1_0$ FePt phase in the annealed film is very important to film magnetic properties and to an understanding of the $L1_0$ FePt phase formation in both cosputtered fcc FePt films and $[Fe/Pt]_n$ multilayer thin films. For example, Ristau and co-workers demonstrated that the volume fraction of the $L1_0$ FePt phase is proportional to the coercivity of polycrystalline FePt films.[3,4] For magnetic recording using FePt thin films or nanoparticles, the $L1_0$ phase fraction, along with its grain/particle size, will determine the maximum recording density.

The fraction of an ordered phase present in a two phase mixture of the disordered and ordered phases can be very difficult to quantify in thin films, and this is especially true for films of the FePt $L1_0$ phase. Quantitative x-ray diffraction is of limited utility because the degree of chemical order of the $L1_0$ phase, as well as its volume fraction, results in similar changes to the relative intensity of the fcc FePt peaks as compared to the superlattice peaks of the $L1_0$ FePt phase. The tetragonal distortion that occurs with ordering is small, and in fine-grained thin films separate quantification of the intensities of the closely related peaks is difficult. For example, there is typically considerable overlap among the fcc {002} peak, the $L1_0$ (002) peak, and the $L1_0$ (200)+(020) peak. Effectively, it is impossible to find an individual peak solely from the disordered fcc phase. Transmission electron microscopy (TEM) has been used successfully to determine the phase fraction of the $L1_0$ FePt phase in highly (111) textured FePt and CoPt films by Ristau and co-workers.[3,4] Their approach is to select individual grains with their 111 zone axis strictly parallel to the electron beam, so that all three $L1_0$ FePt {110} variants potentially nucleated inside one grain are visible and can be illuminated individually in dark field (DF) TEM images. The sum of all illuminated areas in the DF images from superlattice {110} reflections represents all ordered regions, and the ratio of the area of all ordered regions to that of the whole grain gives the $L1_0$ phase fraction of one single grain. Repeating this process for multiple

[a]Electronic mail: bo555252@pegasus.cc.ucf.edu.

TABLE I. A list of the Fe/Pt multilayer films.

Sample ID	Multilayer structure	Period (Å)	Deposition temperature (°C)	Measured composition	Measured thickness (Å)
b1	$[Fe_{22\ Å}Pt_{28\ Å}]_{12}$	50	−50	$Fe_{49.2}Pt_{50.8}$	620
b2	$[Fe_{22\ Å}Pt_{28\ Å}]_{12}$	50	25	$Fe_{49.2}Pt_{50.8}$	620
b3	$[Fe_{22\ Å}Pt_{28\ Å}]_{12}$	50	150	$Fe_{49.2}Pt_{50.8}$	620
b4	$[Fe_{22\ Å}Pt_{28\ Å}]_{12}$	50	200	$Fe_{49.2}Pt_{50.8}$	620
b5	$[Fe_{22\ Å}Pt_{28\ Å}]_{12}$	50	250	$Fe_{49.2}Pt_{50.8}$	620
c1	$[Fe_{5\ Å}Pt_{6.4\ Å}]_{48}$	11.4	250	$Fe_{47.1}Pt_{52.9}$	515
c2	$[Fe_{10\ Å}Pt_{12.8\ Å}]_{24}$	22.8	250	$Fe_{47.1}Pt_{52.9}$	515
c3	$[Fe_{20\ Å}Pt_{25.6\ Å}]_{12}$	45.6	250	$Fe_{47.1}Pt_{52.9}$	515
c4	$[Fe_{40\ Å}Pt_{51.3\ Å}]_{6}$	91.3	250	$Fe_{47.1}Pt_{52.9}$	515
c5	$[Fe_{80\ Å}Pt_{102.6\ Å}]_{3}$	182.6	250	$Fe_{47.1}Pt_{52.9}$	515

grains determines the $L1_0$ phase fraction of one sample. It can be seen that this method is very laborious even for highly (111) textured films with large grains (such as films annealed at 700 °C). For films with a much smaller grain size or without such strong texture, the application of this technique becomes even more difficult.

This paper reports the use of hollow cone dark field (HCDF) TEM imaging to quantitatively determine the phase fraction of $L1_0$ FePt and fcc FePt in the annealed $[Fe/Pt]_n$ films. Two sets of multilayer films with varying deposition temperature and periodicity were examined using the technique.

II. EXPERIMENTS

Two sets of $[Fe/Pt]_n$ multilayer films with varying deposition temperature and periodicity, as listed in Table I, were prepared to study the formation of $L1_0$ FePt phase in multilayer thin films. All samples studied have similar Fe/Pt compositions, close to the stoichiometric $L1_0$ composition of 50 at. % Fe. All samples were sputtered onto Si (100) substrates having a surface layer of 100 nm of thermally grown SiO_2. The deposition rate for Pt was 0.31 Å/s and that for Fe was 0.48 Å/s, as determined by Rutherford backscattering spectroscopy. All depositions were performed in 4 mTorr of Ar+3% H_2. A chamber pressure in the 10^{-8} Torr range was obtained prior to film deposition. The film samples were annealed in a modified tube furnace in 1 atm of flowing Ar +5% H_2 process gas.[5] The successful deposition of the intended multilayer structure was confirmed by low angle x-ray diffraction previously reported.[5,6] All of the as-deposited samples were magnetically "soft," consistent with the absence of the high anisotropy $L1_0$ phase.[5] The compositional gradients in the as-deposited samples were observed to be homogenized during relatively low temperature annealing, 350 °C, during which the disordered fcc FePt alloy was formed. While evidence of $L1_0$ phase nucleation has been observed in the samples annealed at 350 °C,[7] this study focuses on samples annealed at a higher temperature, 400 °C, in which a more substantial fraction of the sample has been converted to the $L1_0$ phase.

The technique described in this paper requires a very thin layer of FePt film for TEM examination, as to avoid the overlap of multiple grains in the thickness direction and to mimimize dynamical scattering effects. A recently reported back-etch method was used to prepare such required TEM membranes. This sample preparation method involves initially thinning the Si substrate with $HF+HNO_3$ solution and subsequent thinning with low angle ion milling[8,9] to make the FePt film transparent to light. The optical transparency of such metallic films indicates a thickness below 20 nm. The microscopy was performed in a Tecnai F 30 microscope with a field emission gun operating at 300 kV and below. Magnetic properties were measured with an alternating gradient force magnetometer (Princeton Measurements Corp., Micro-Mag model 2900) with a maximum field of 20 kOe. The image processing and analysis were conducted with the IMAGEJ software provided by the National Institutes of Health.

III. METHOD FOR THE $L1_0$ FePt PHASE VOLUME FRACTION QUANTIFICATION

The ordered $L1_0$ FePt phase has a tetragonal structure slightly distorted from that of the disordered fcc phase. In the disordered phase, each position is occupied by Fe and Pt atoms with the same probability. In the ordered $L1_0$ phase, however, the Fe and Pt atomic layers occupy the structure alternatively along the ⟨001⟩ direction. Consequently, the c axis of the $L1_0$ structure is slightly smaller than that of the a and b axes. A typical selected area diffraction pattern (SADP) of a film containing both the ordered $L1_0$ and disordered fcc FePt phases is shown in Fig. 1. Both phases share the same fundamental reflections such as 111, 200, 220, 311,

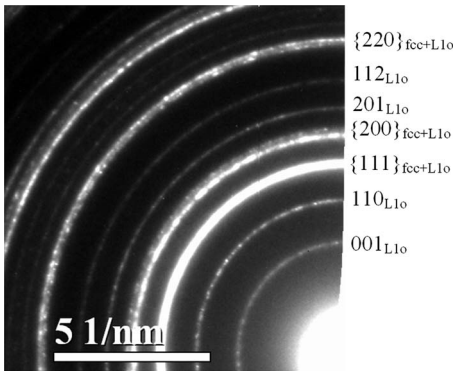

FIG. 1. Portion of a TEM SADP of a film containing both ordered $L1_0$ and disordered fcc FePt phases.

TABLE II. The reflections along with the contributing planes.

Reflections	Planes contributing the reflection
001_{L1_0}	$(001)_{L1_0}$
110_{L1_0}	$(110)_{L1_0}$
$\{200\}_{fcc+L1_0}$	$(200)_{fcc}$, $(020)_{fcc}$, $(002)_{fcc}$, $(200)_{L1_0}$, $(020)_{L1_0}$, $(002)_{L1_0}$
201_{L1_0}	$(201)_{L1_0}$
112_{L1_0}	$(112)_{L1_0}$
$\{220\}_{fcc+L1_0}$	$(220)_{fcc}$, $(202)_{fcc}$, $(022)_{fcc}$, $(220)_{L1_0}$, $(202)_{L1_0}$, $(022)_{L1_0}$

etc. Among these, the 200 and 220 rings are split into two rings due to the reduction in symmetry of the $L1_0$ structure compared to that of the fcc phase. However, the distortion is so small that the split rings cannot be separated effectively. Therefore, for simplicity, the split rings will be handled together and labeled as $\{200\}_{fcc+L1_0}$, $\{220\}_{fcc+L1_0}$, etc. The remaining reflections in Fig. 1 are the superlattice reflections solely from the $L1_0$ phase and labeled as 001_{L1_0}, 110_{L1_0}, 201_{L1_0}, 112_{L1_0}, etc. Table II lists the planes contributing to the reflections. It should be noted that the multiplicity of 001_{L1_0} and 110_{L1_0} is only 1/3 that of the $\{200\}_{fcc+L1_0}$ or $\{220\}_{fcc+L1_0}$.

The HCDF TEM technique is to form a DF TEM image using one or more whole rings, excluding the direct beam and other reflections. For example, HCDF(001_{L1_0}) indicates the DF TEM image using the 001 superlattice ring of the $L1_0$ FePt phase. The grains illuminated in HCDF(001_{L10}) indicate all the $L1_0$ FePt grains having (001) planes parallel to the electron beam. Correspondingly, the illuminated grains in HCDF($\{200\}_{fcc+L1_0}$) represent all the fcc and $L1_0$ phase grains with their (200), (020), and (002) planes parallel to the electron beam.

The technique introduced in this paper is based on the measurement of the illuminated grain areas in HCDF TEM images generated from specific diffraction rings. In theory, for polycrystalline samples consisting of a single layer of randomly oriented grains (without strong texture), the volume fraction of the $L1_0$ FePt phase (f_{L1_0}) can be decided by

$$f_{L1_0} = \frac{3 \times \text{area\_HCDF}(001_{L1_0})}{\text{area\_HCDF}(\{200\}_{L1_0+fcc})}, \quad (1)$$

where the area_HCDF( ) function is defined as the total illuminated grain area in the HCDF TEM images from the specific reflection(s) or planes in the brackets.

For quantitative implementation of Eq. (1), the assumptions implicitly used in derivation need to be considered. One such assumption is that for the $L1_0$ FePt phase, the $(001)_{L1_0}$ oriented grains illuminated in HCDF(001_{L1_0}) are also similarly illuminated as $(002)_{L1_0}$ in HCDF($\{200\}_{fcc+L1_0}$), as stated by

$$\text{area\_HCDF}(002_{L1_0}) = \text{area\_HCDF}(001_{L1_0}). \quad (2)$$

Another implicit assumption of Eq. (1) is that 200_{L1_0}, 020_{L1_0}, and 002_{L1_0} planes have the same probability to be illuminated, as stated by

$$\text{area\_HCDF}(200_{L1_0} + 020_{L1_0} + 002_{L1_0}) = 3 \times \text{area\_HCDF}(002_{L1_0}). \quad (3)$$

This assumption holds true for random or slightly oriented samples but may not be appropriate for highly textured films. The nature of the texture in thin films is that certain preferred planes (i.e., 111) lie in the film plane, and the film may possess a distribution of randomly oriented grains and textured grains. During TEM examination, the TEM membrane can be tilted away from the texture axis so that the textured grains do not satisfy the Bragg reflection.[10,11] In the tilted orientation (10° away in this paper), the illuminated grains can thus be assumed to be randomly oriented. The volume fraction of the ordered phase present in the sample can then be calculated if it is assumed that the ordered fraction of the randomly oriented grains is equal to the ordered fraction of the textured grains or it may alternatively be assumed that the volume fraction of textured grains is negligible. For the work presented here, the plan view samples were tilted away from the texture direction to minimize the potential influence of textured grains, although no detectable textures were found for the samples.

Another practical problem is to distinguish closely related rings for DF imaging, specifically the $\{200_{L1_0+fcc}\}$ ring and the $112_{L1_0}+201_{L1_0}$ rings. At the normal operating voltage (300 kV) of the microscope used in this study (Tecnai F30), the available objective apertures were too large to select only the $\{200_{Lcc+fcc}\}$ reflection while excluding neighbor reflections. Two solutions were developed and used and are described in detail below.

The first solution is to reduce the beam voltage to 100 kV, which increases the relative size of SADP to the objective aperture. While this improvement is insufficient to allow the $\{200_{Lcc+fcc}\}$ ring to be individually selected, it does allow individual selection of the $112_{L1_0}+201_{L1_0}$. Equation (4) is then used to calculate the total illuminated grain area of the $\{200_{L1_0+fcc}\}$ ring as the difference between the illuminated grain area of the combined $\{200_{L1_0+fcc}\}$ and $112_{L1_0}+201_{L1_0}$ rings and illuminated grain area of the $112_{L1_0}+201_{L1_0}$ ring,

$$\text{area\_HCDF}(\{200\}_{L1_0+fcc}) = \text{area\_HCDF}(\{200_{L1_0+fcc}\} + 201_{L1_0} + 112_{L1_0}) - \text{area\_HCDF}(201_{L1_0} + 112_{L1_0}). \quad (4)$$

The determination of the area of illuminated grains in a DF TEM image requires the accurate separation of the illuminated grains from the background based on contrast (i.e., intensity). Because of the uniform (not bimodal) distribution of grain contrast present in the images, the selection of an intensity level to distinguish the illuminated grains from the background intensity is subject to arbitrary variation by the operator, and hence uncertainty in the illuminated grain area in the image and potential error in the ordered fraction calculated. To eliminate this potential source of error in the calculation of the ordered fraction, only the HCDF($\{200\}_{L1_0+fcc}+201_{L1_0}+112_{L1_0}$) image is manually contrast selected to identify the illuminated grains. All other HCDF images [from the (001_{L1_0}) ring and from the $(201_{L1_0}$

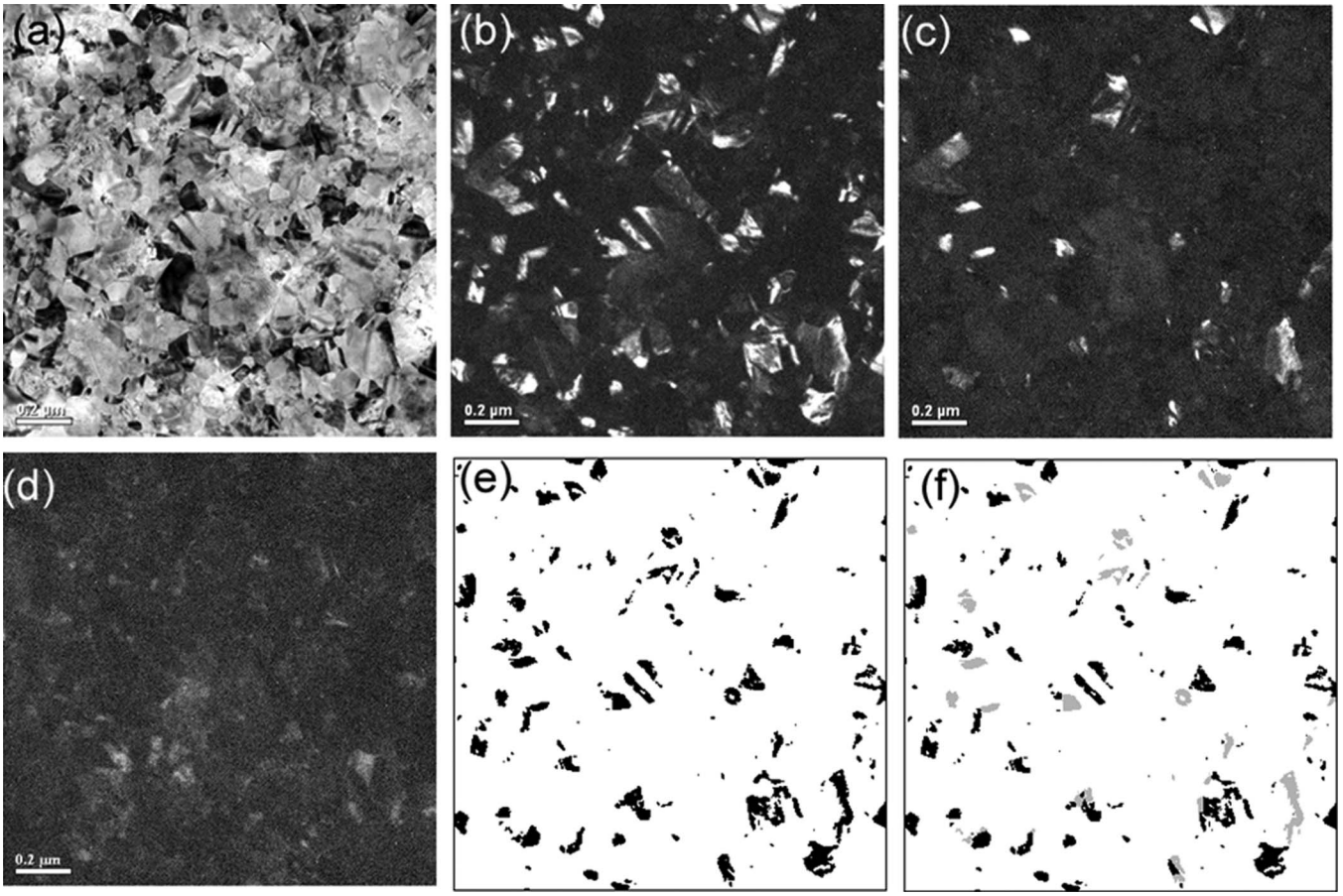

FIG. 2. The (a) bright field, (b) HCDF($\{200_{L1_0+\mathrm{fcc}}\}+201_{L1_0}+112_{L1_0}$), (c) HCDF($001_{L1_0}$), (d) HCDF($201_{L1_0}+112_{L1_0}$), (e) contrast selected HCDF($\{200_{L1_0+\mathrm{fcc}}\}+201_{L1_0}+112_{L1_0}$), and (f) processed binary TEM images of a typical multilayer sample annealed at 500 °C for 30 min. In the processed image, the light gray level grains indicate $L1_0$ phase grains with 001 planes illuminated, and the dark grains indicates all fcc grains with {200} family planes illuminated, as well as the $L1_0$ grains with 200 or 020 planes illuminated.

$+112_{L1_0}$) ring] are projected onto the contrast selected HCDF($\{200\}_{L1_0+\mathrm{fcc}}+201_{L1_0}+112_{L1_0}$) binary image and areas calculated based only on grains present in the initial HCDF($\{200\}_{L1_0+\mathrm{fcc}}+201_{L1_0}+112_{L1_0}$) image. In this way, all the illuminated grains experienced the same initial contrast selection uncertainty, and the relative uncertainty of area fractions is unaffected.

Details of the image processing will be described below with a specific example. For each TEM field of view, three HCDF images, HCDF($\{200\}_{L1_0+\mathrm{fcc}}+201_{L1_0}+112_{L1_0}$), HCDF($201_{L1_0}+112_{L1_0}$), and HCDF($001_{L1_0}$), were obtained as above. Figure 2 shows a bright field and the three HCDF TEM images of a typical view. The following processing steps were used to determine the volume fraction of the $L1_0$ FePt phase present.

(1) The HCDF($\{200_{L1_0+\mathrm{fcc}}\}+201_{L1_0}+112_{L1_0}$) image, Fig. 2(b), was contrast selected to separate illuminated grains from the background. This contrast selected image is shown as Fig. 2(e). A comparison of HCDF($\{200_{L1_0+\mathrm{fcc}}\}+201_{L1_0}+112_{L1_0}$), HCDF($201_{L1_0}+112_{L1_0}$), and HCDF($001_{L1_0}$) reveals that the illumi-

TABLE III. The intensity evaluation of diffraction beams of $L1_0$ FePt.

Reflections *hkl*	Structure factor F_{hkl} (Å)	Extinction distance ξ_g (Å)	Intensity *I* (%)		
			S=1	*S*=0.8	*S*=0.7
0 0 1	30.1	286.89	79.0	50.6	48.1
1 1 0	18.8	459.32	39.9	25.6	21.2
2 0 0	24.3	354.73	60.0	60.0	60.0
0 0 2	23.2	372.07	55.9	55.9	55.9
2 0 1	9.8	880.98	12.2	7.8	6.1
1 1 2	8.5	1015.64	9.3	5.9	4.6
2 2 0	15.7	548.67	29.4	29.4	29.4
2 0 2	15.4	561.62	28.2	28.2	28.2

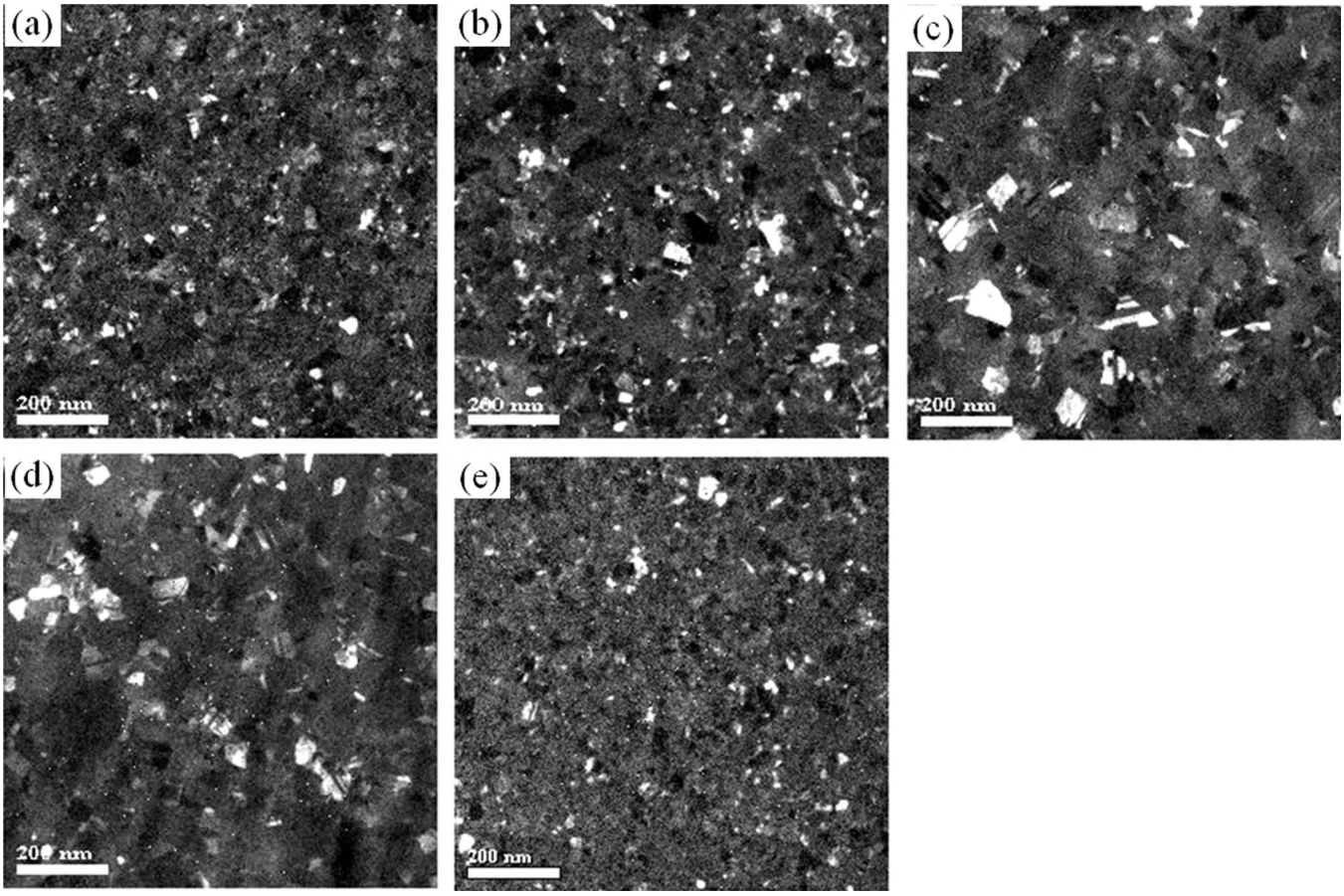

FIG. 3. [(a)–(e)] The HCDF TEM images from $L1_0$ 001 and 110 superlattice reflections of samples b1–b5 annealed at 400 °C for 30 min, respectively.

nated grains in HCDF($201_{L1_0}+112_{L1_0}$), Fig. 2(d), have a much weaker intensity. This is not coincidental, as will be discussed in detail later. The lower intensity of the ($201_{L1_0}+112_{L1_0}$) orientated grains in the HCDF($\{200_{L1_0+\mathrm{fcc}}\}+201_{L1_0}+112_{L1_0}$) image allows them to be separated out from the ($\{200\}_{L1_0+\mathrm{fcc}}$) grains by contrast using the HCDF($201_{L1_0}+112_{L1_0}$) image as a guide to the appropriate contrast level to be used. The effectiveness of the approach can be clearly confirmed by a comparison of Figs. 2(d) and 2(e).

(2) The enlarged contrast selected binary image, i.e., Fig. 2(e) in the example, was printed on a transparency film, and the enlarged HCDF(001_{L1_0}) [Fig. 2(b)] image was printed on a paper. The same magnifications are used.

(3) The next step is to overlap the printed transparent films, showing the $\{200\}_{\mathrm{fcc}+L1_0}$ illuminated grains, onto the printed paper showing the $(001)_{L1_0}$ illuminated grains. On the transparency film all the $(001)_{L1_0}$ grains are circled out. The 001_{L1_0} grains are identified by the fact that they are illuminated on both the transparency film and paper. This step accomplishes the projection of the $(001)_{L1_0}$ illuminated grains onto the $\{200\}_{\mathrm{fcc}+L1_0}$ illuminated grain.

(4) The contrast level of the circled 001_{L1_0} grains is changed to a different gray level (a light gray level in the example) with the software, as shown in Fig. 2(f). Therefore, the light gray level in Fig. 2(f) shows 001_{L1_0} grains, while the light gray level and dark gray level together give $\{200_{L1_0+\mathrm{fcc}}\}$ grains. The area fraction of 001_{L1_0} grains to $\{200_{L1_0+\mathrm{fcc}}\}$ grains gives the volume fraction of the $L1_0$ FePt phase based on Eq. (1). The volume fractions of different gray levels were measured with the IMAGE J software.

(5) For each sample, multiple views (usually above 5) are necessary to get an acceptable standard deviation (<5%).

A second solution is based on Eq. (5) and a modified technique applicable to samples processed at lower temperature (≤500 °C). In this approach, only two HCDF images, HCDF($001_{L1_0}+110_{L1_0}$) and HCDF($\{200+220\}_{L1_0+\mathrm{fcc}}+112_{L1_0}+201_{L1_0}$), are required at each view, and it is assumed that contrast alone can be used to eliminate the 112_{L1_0} and 201_{L1_0} oriented grains from inclusion in the $\{200+220\}_{L1_0+\mathrm{fcc}}$ grain area determination.

$$f_{L1_0}=\frac{3\times\ \mathrm{area\_HCDF}(001+110)_{L1_0})}{\mathrm{area\_HCDF}(\{200+220\}_{L1_0+\mathrm{fcc}})}. \tag{5}$$

This assumption has been confirmed as valid by both TEM image observations and calculations of scattered electron intensity at both 100 and 300 kV. During implementation of the first solution (described above) it was observed that the illuminated grains from 201_{L1_0} and 112_{L1_0} reflections had much lower intensities than those from 001_{L1_0}, 110_{L1_0},

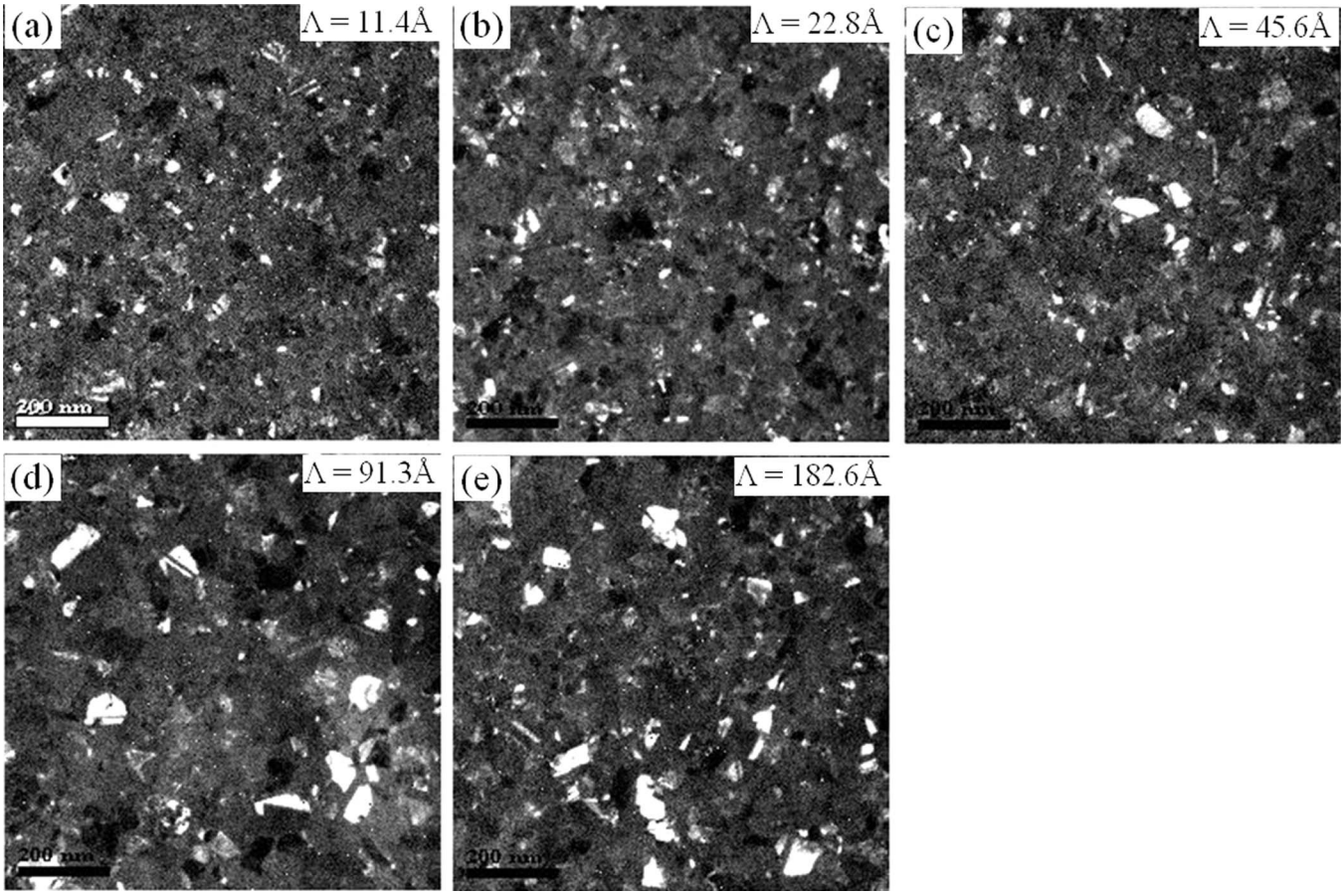

FIG. 4. [(a)–(e)] HCDF TEM images of samples c1–c5 annealed at 400 °C for 30 min from 001 and 110 superlattice diffraction rings.

and $\{200+220\}_{\text{fcc}+L1_0}$ reflections. This observation spanned a total of more than 50 views and 10 samples annealed at or below 500 °C. A simple diffraction intensity evaluation of the different reflections using Howie–Whelan equations was conducted[12] and the results are shown in Table III, which are very consistent with the experimental observations. For films annealed at or below 500 °C, the $L1_0$ FePt phase has a relatively lower long range order parameter (S) and a much lower illumination intensity from the 201_{L1_0} and 112_{L1_0} reflections is induced by their small scattering abilities and their reduced extent of chemical order. Accordingly, an appropriate selection of contrast level to distinguish the illuminated grains from the background can also be readily used to distinguish the $\{200+220\}_{\text{fcc}+L1_0}$ illuminated grains from the 201_{L1_0} and 112_{L1_0} illuminated grains, without reference to a separate HCDF($201_{L1_0}+112_{L1_0}$) image. This minimizes the effort required for measurements, as only two HCDF images are now required to calculate the ordered fraction present. The TEM image acquisition and processing otherwise follow the same procedures as described for the first solution above.

It is worth noting that for films annealed at high temperature (i.e., 700 °C), the films may be highly ordered with S close to 1 and correspondingly, the intensity of $(201+112)_{L1_0}$ illuminated grains in the DF image may be comparable to that of $(001+110)_{L1_0}$ and $\{200+220\}_{L1_0+\text{fcc}}$. In this case, the use of contract to distinguish the grains cannot be used and the third HCDF image is required.

IV. RESULTS AND DISCUSSION

Both sets of samples were annealed at 400 °C for 30 min. The magnetic properties and microstructure characterization of these samples annealed at other temperatures have been reported elsewhere,[5,6] whereas this work focuses on the $L1_0$ volume fraction quantification. The $L1_0$ FePt phase grain size, volume fraction, and magnetic properties of annealed films were examined to study the influence of deposition temperature and periodicity.

The influence of substrate temperature on the $L1_0$ phase grain size (samples "b1," "b2," "b3," "b4," and "b5") is shown in Fig. 3. It can be seen that the samples deposited at low temperature [sample b1, Fig. 3(a)] and high temperature [sample b5, Fig. 3(e)] have a smaller grain size for the $L1_0$ phase. Samples b3 and b4 have relatively large grains, and sample b2 has an intermediate size compared to four other samples. Figure 4 shows the HCDF TEM images obtained from the 001 and 110 $L1_0$ FePt superlattice reflections of samples "c1," "c2," "c3," "c4," and "c5" as annealed. The grain size of $L1_0$ FePt is observed to generally increase with the increase in bilayer period.

The measured volume fraction of the $L1_0$ FePt phase using the techniques described above is shown in Figs. 5(a) and 5(b), respectively. The influence of deposition temperature on the $L1_0$ FePt volume fraction can be seen in Fig. 5(a). The samples deposited at colder temperature (−50 °C) and higher temperature (250 °C) have a smaller volume fraction.

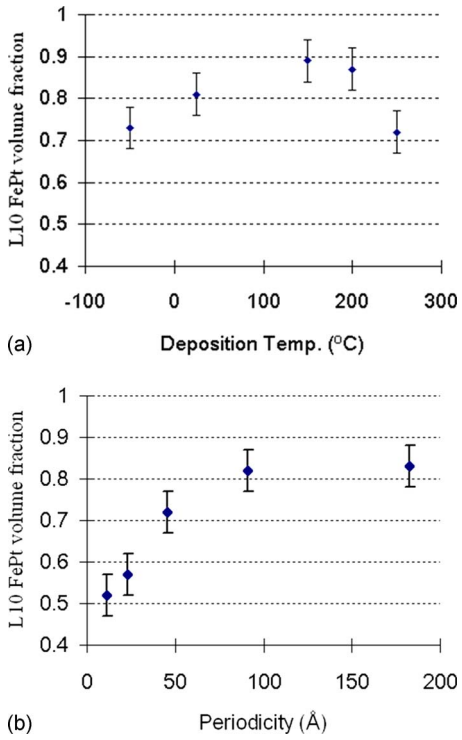

FIG. 5. (Color online) The measured volume fraction of $L1_0$ FePt phase vs (a) the deposition temperature and (b) the periodicity of two sets of samples annealed at 400 °C for 30 min.

The samples that provide the maximum $L1_0$ volume fractions are those deposited at 150 and 200 °C. Figure 5(b) shows the influence of layer periodicity on the $L1_0$ phase volume fraction. For samples with periodicity smaller than 5 nm, the $L1_0$ phase volume fraction drops quickly with the decrease in periodicity. The volume fraction of the $L1_0$ phase tends to reach a plateau for samples with periodicity higher than ~10 nm.

The in-plane magnetic properties of the annealed samples were also measured. The films were found to have no crystallographic texture (by TEM); thus we expect the in-plane loops to be representative of an isotropic distribution of the magnetic easy axis of the $L1_0$ phase grains. The results show that both the deposition temperature and periodicity of films have a great influence on the magnetic property. Figure 6(a) shows the *M-H* loops of samples b1–b5. Figure 6(b) shows the estimated coercivity versus the deposition temperature for these samples (it should be noted that the maximum field used for these measurements, 20 kOe, may be insufficient to fully saturate these samples). The sample deposited at 150 °C has the maximum coercivity of 11.2 kOe, while those deposited at lower and higher temperatures (−50 and 250 °C, respectively) have a reduced coercivity. Figure 7(a) shows the *M-H* loops of samples c1–c5. Figure 7(b) shows the estimated coercivity versus the periodicity for these samples. It is obvious that the coercivity increases with the increase in periodicity.

Figure 8 shows the in-plane coercivity versus the measured volume fraction of the $L1_0$ FePt phase for the two sets of samples. The fitted lines indicate that the coercivity of the annealed samples generally increases with the volume fraction for samples in each group, consistent with previous reports.[3,4] Figure 8 also shows that each set of samples has a different rate of coercivity increase with the $L1_0$ phase fraction, suggesting differences in microstructure and/or extent of ordering between the two sample sets.

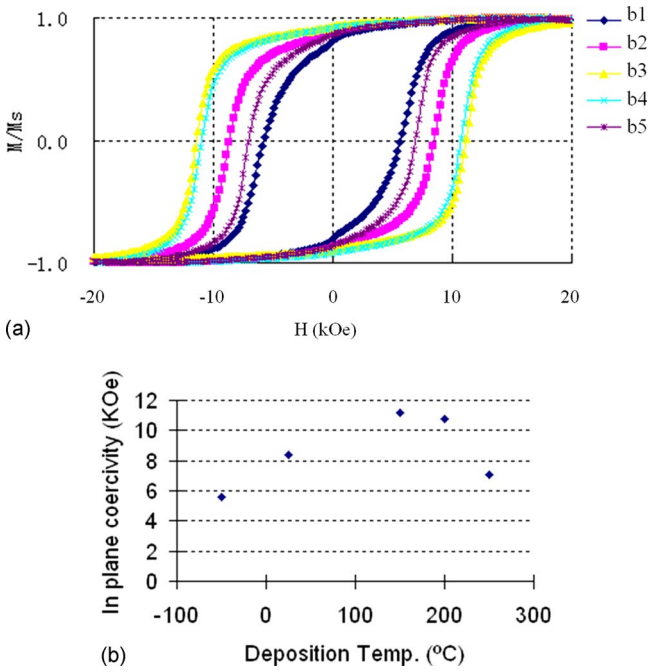

FIG. 6. (Color online) (a) The *M-H* curves and (b) the in-plane H_c vs deposition temperature for samples b1–b5. All samples were annealed at 400 °C for 30 min.

A comparison of the above results indicates that a correlation between the $L1_0$ phase fraction, grain size, and magnetic properties is followed. Generally, samples with high

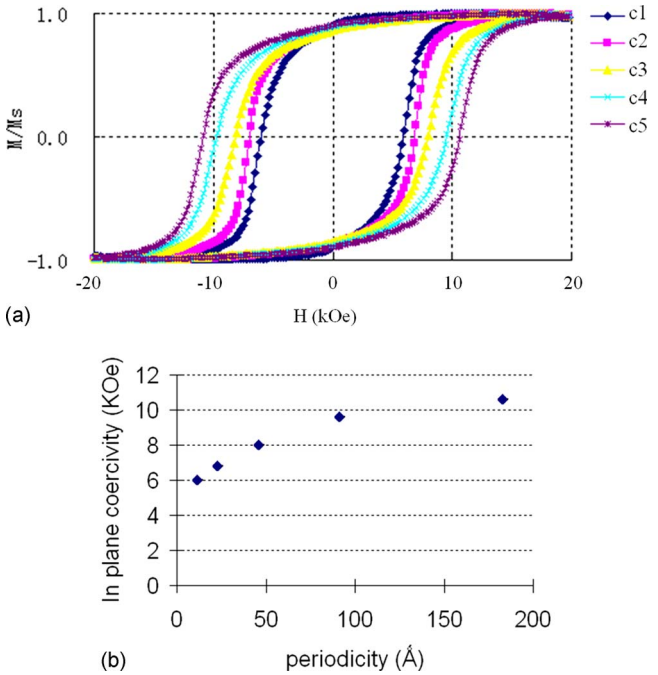

FIG. 7. (Color online) (a) The *M-H* curves and (b) the in-plane H_c vs periodicity for samples c1–c5. All samples were annealed at 400 °C for 30 min.

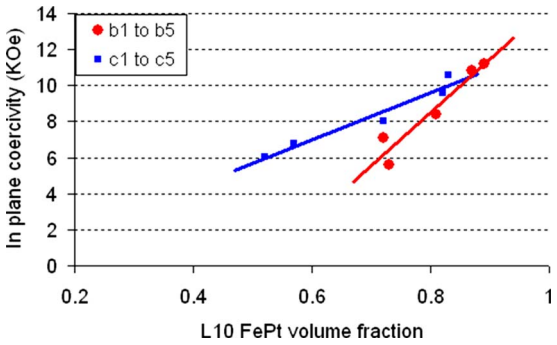

FIG. 8. (Color online) The in-plane coercivity vs the $L1_0$ FePt volume fraction of two sets of samples with varying substrate temperature (b1–b5) and bilayer periodicity (c1–c5). All samples were annealed at 400 °C for 30 min.

coercivity also possess large value of the $L1_0$ phase fraction and larger grain size. This result may indicate that the grain growth of the $L1_0$ FePt phase, at the expense of disordered fcc FePt phase, is an important mechanism to increase the $L1_0$ phase fraction, and that a large fraction of the $L1_0$ FePt phase in the polycrystalline annealed film results in an increased coercivity. While it is generally expected that an increasing grain size and a reduction in film defects will eventually result in a decrease in coercivity, this limiting case was not observed within the experiments above.

V. CONCLUSIONS

A method based on the HCDF TEM imaging is introduced to quantitatively determine the phase fraction of the $L1_0$ FePt and fcc FePt in the annealed films. Two sets of annealed $[Fe/Pt]_n$ multilayer films with varying deposition temperature and periodicity were examined. It was found that both the deposition temperature and periodicity strongly influence the film structure and film magnetic properties. A correlation between the $L1_0$ phase volume fraction, grain size, and magnetic properties was observed.

[1]R. Skomski, J. Phys.: Condens. Matter **15**, R841 (2003).
[2]V. Raghavendra Reddy, S. Kavita, and A. Gupta. J. Appl. Phys. **99**, 113906 (2006).
[3]K. Barmak, R. A. Ristau, K. R. Coffey, M. A. Parker, and J. K. Howard, J. Appl. Phys. **79**, 5330 (1996).
[4]R. A. Ristau, K. Barmak, L. H. Lewis, K. R. Coffey, and J. K. Howard, J. Appl. Phys. **86**, 4527 (1999).
[5]B. Yao and K. R. Coffey, J. Magn. Magn. Mater. **320**, 559 (2008).
[6]B. Yao and K. R. Coffey, J. Appl. Phys. **103**, 07E107 (2008).
[7]B. Yao and K. R. Coffey, J. Electron Microsc. **57**, 189 (2008).
[8]B. Yao and K. R. Coffey, J. Electron Microsc. **57**, 47 (2008).
[9]B. Yao, R. V. Petrova, R. R. Vanfleet, and K. R. Coffey J. Electron Microsc. **56**, 209 (2007).
[10]L. Tang and D. E. Laughlin, J. Appl. Crystallogr. **29**, 411 (1996).
[11]L. Tang and D. E. Laughlin, J. Appl. Crystallogr. **29**, 419 (1996).
[12]D. B. Williams and C. C. Barry, *Transmission Electron Microscopy, A Textbook for Materials Science* (Plenum, New York, 1996).